Atmospheric
Chemistry
and Physics

Impacts of aerosol direct effects on tropospheric ozone through changes in atmospheric dynamics and photolysis rates

Jia Xing[1,*], **Jiandong Wang**[1,*], **Rohit Mathur**[2], **Shuxiao Wang**[1], **Golam Sarwar**[2], **Jonathan Pleim**[2], **Christian Hogrefe**[2], **Yuqiang Zhang**[2], **Jingkun Jiang**[1], **David C. Wong**[2], and **Jiming Hao**[1]

[1]State Key Joint Laboratory of Environmental Simulation and Pollution Control, School of Environment, Tsinghua University, Beijing 100084, China
[2]The U.S. Environmental Protection Agency, Research Triangle Park, NC 27711, USA
[*]These authors contributed equally to this work.

Correspondence to: Shuxiao Wang (shxwang@tsinghua.edu.cn)

Abstract. Aerosol direct effects (ADEs), i.e., scattering and absorption of incoming solar radiation, reduce radiation reaching the ground and the resultant photolysis attenuation can decrease ozone (O_3) formation in polluted areas. One the other hand, evidence also suggests that ADE-associated cooling suppresses atmospheric ventilation, thereby enhancing surface-level O_3. Assessment of ADE impacts is thus important for understanding emission reduction strategies that seek co-benefits associated with reductions in both particulate matter and O_3 levels. This study quantifies the impacts of ADEs on tropospheric ozone by using a two-way online coupled meteorology and atmospheric chemistry model, WRF-CMAQ, using a process analysis methodology. Two manifestations of ADE impacts on O_3 including changes in atmospheric dynamics (ΔDynamics) and changes in photolysis rates (ΔPhotolysis) were assessed separately through multiple scenario simulations for January and July of 2013 over China. Results suggest that ADEs reduced surface daily maxima 1 h O_3 (DM1O_3) in China by up to 39 µg m^{-3} through the combination of ΔDynamics and ΔPhotolysis in January but enhanced surface DM1O_3 by up to 4 µg m^{-3} in July. Increased O_3 in July is largely attributed to ΔDynamics, which causes a weaker O_3 sink of dry deposition and a stronger O_3 source of photochemistry due to the stabilization of the atmosphere. Meanwhile, surface OH is also enhanced at noon in July, though its daytime average values are reduced in January. An increased OH chain length and a shift towards more volatile organic compound (VOC)-limited conditions are found due to ADEs in both January and July. This study

suggests that reducing ADEs may have the potential risk of increasing O_3 in winter, but it will benefit the reduction in maxima O_3 in summer.

1 Introduction

Photochemistry in the atmosphere is a well-known source of tropospheric ozone (O_3) (e.g., Haagen-Smit and Fox, 1954) and is determined by ambient levels of O_3 precursors (i.e., NO$_x$ and VOC) and photolysis rates, which are largely influenced by meteorological factors such as solar irradiance and temperature. It is well known that aerosols influence radiation through light scattering and absorption, thereby modulating atmospheric radiation and temperature. These aerosol direct effects (ADEs) can then impact thermal and photochemical reactions leading to the formation of O_3 (Dickerson et al., 1997). Recent studies suggest that the aerosol-induced reduction in solar irradiance leads to lower photolysis rates and less O_3 (e.g., Benas et al., 2013), and therefore extensive aerosol reductions, particularly in developing regions such as in East Asia, may pose a potential risk by enhancing O_3 levels (Bian et al., 2007; Anger et al., 2016; Wang et al., 2016). For example, Wang et al. (2016) found that because of ADEs, the surface 1 h maximum ozone (noted as DM1O_3) was reduced by up to 12 % in eastern China during the EAST-AIRE campaign, suggesting that the benefits of PM$_{2.5}$ reductions may be partially offset by increases in ozone associated with reducing ADEs.

Ambient O_3 levels are influenced by several sources and sinks. The modulation of photolysis rates by ADEs is only one manifestation of ADEs impacts on O_3. In addition, ADEs modulate the temperature (e.g., Hansen et al., 1997; Mitchell et al., 1995), atmospheric ventilation (e.g., Jacobson et al., 2007; Mathur et al., 2010), cloud and rainfall (e.g., Albrecht, 1989; Liou and Ou, 1989; Twomey, 1977), which also influence the O_3 concentrations. Therefore, ADEs can impact air quality through multiple pathways and process chains (Jacobson, 2002, 2010; Jacobson et al., 2007; Wang et al., 2014; Xing et al., 2015a; Ding et al., 2016). For example, Xing et al. (2015a) suggested that the O_3 response to ADEs is largely contributed by the increased precursor concentrations which enhance the photochemical reaction, presenting an overall positive response of O_3 to ADEs by up to 2–3 % in eastern China. The assessment of a separate contribution from individual processes is necessary for fully understanding how ADEs impact O_3.

In China, atmospheric haze is currently one of the most serious environmental issues of concern. Over the next decade, the national government plans to implement stringent control actions aimed at lowering the $PM_{2.5}$ concentrations (Wang et al., 2017). Ideas on whether such extensive aerosol controls will enhance O_3 and oxidation capacity needs to be carefully assessed and quantified. Many studies suggest that aerosols may have substantial impacts on ozone through heterogeneous reactions including hydrolysis of N_2O_5, irreversible absorption of NO_2 and NO_3, as well as the uptake of HO_2 (Tang et al., 2004; Tie et al., 2005; Liao and Seinfeld, 2005; Pozzoli et al., 2008; Li et al., 2011; Xu et al., 2012; Lou et al., 2014). While our model contains comprehensive treatment of the heterogeneous hydrolysis of N_2O_5 (Davis et al., 2008; Sarwar et al., 2012, 2014), we have not quantified its impacts on ozone in this study. However, ADE impacts on ozone have not been well evaluated previously. Accurate assessment of the multiple ADE impacts is a prerequisite for accurate policy decision. The process analysis (PA) methodology is an advanced probing tool that enables quantitative assessment of integrated rates of key processes and reactions simulated in the atmospheric model (Jang et al., 1995; Zhang et al., 2009; Xu et al., 2008; Liu et al., 2010; Xing et al., 2011). In this study, we apply the PA methodology in the two-way coupled meteorology and atmospheric chemistry model, i.e., the Weather Research and Forecasting (WRF) model coupled with the Community Multiscale Air Quality (CMAQ) model developed by U.S. Environmental Protection Agency (Pleim et al., 2008; Mathur et al., 2010, 2014; Wong et al., 2012; Yu et al., 2014; ; Xing et al., 2015b) to examine the process chain interactions arising from ADEs and quantify their impacts on O_3 concentration.

The paper is organized as following. A brief description of the model configuration, scenario design and PA method is presented in Sect. 2. The O_3 response to ADEs is discussed in Sect. 3.1. PA analyses are discussed in Sect. 3.2–3.3. The summary and conclusion is provided in Sect. 4.

2   Method

2.1   Modeling system

The two-way coupled WRF-CMAQ model has been detailed and fully evaluated in our previous papers (Wang et al., 2014; Xing et al., 2015a, b). The meteorological inputs for WRF simulations were derived from the NCEP FNL (Final) Operational Global Analysis data which has 1° spatial and 6 h temporal resolution. NCEP Automated Data Processing (ADP) Operational Global Surface Observations were used for surface reanalysis and four-dimensional data assimilation. We have tested and chosen the proper strength of nudging coefficients; i.e., $0.00005\,\mathrm{s}^{-1}$ is used for nudging both u/v-wind and potential temperature and $0.00001\,\mathrm{s}^{-1}$ is used for nudging the water vapor mixing ratio to improve model performance without dampening the effects of radiative feedbacks (Hogrefe et al., 2015; Xing et al., 2015b). In the model version used here, concentrations of gaseous species and primary and secondary aerosols are simulated by using Carbon Bond 05 gas-phase chemistry (Sarwar et al., 2008) and the sixth-generation CMAQ modal aerosol model (AERO6) (Appel et al., 2013). The aerosol optical properties were estimated by the coated-sphere module (i.e., BHCOAT; Bohren and Huffman, 1983) based on simulated aerosol composition and size distribution (Gan et al., 2015). In the coupled model, the estimated aerosol optical properties are fed to the RRTMG radiation module in WRF, thus updating the simulated atmospheric dynamics which then impact the simulated temperature, photolysis rate, transport, dispersion, deposition, cloud mixing and removal of pollutants. Due to large uncertainties associated with the representation of aerosol impacts on cloud droplet number and optical thickness, the indirect radiative effects of aerosols are not included in the current calculation.

The gridded emission inventory and initial and boundary conditions are consistent with our previous studies (Zhao et al., 2013a, b; Wang et al., 2014), while the simulated domain is extended slightly to cover all of China, as shown in Fig. 1. A better model performance in the simulation of dynamic fields including total solar radiation, planetary boundary layer (PBL) height data as well as $PM_{2.5}$ concentrations was suggested after the inclusion of ADEs (Wang et al., 2014). In this study, the model performance in the simulation of O_3 will be evaluated through the comparison with observations from 74 cities across China from the China National Urban Air Quality Real-time Publishing Platform (http://113.108.142.147:20035/emcpublish/). The simulation period is selected as 1 to 31 January and 1 to 31 July in 2013 to represent winter and summer conditions, respectively. Five regions are selected for analysis, including the Jing-Jin-Ji area (denoted JJJ), the Yangzi River Delta (denoted YRD), the Pearl River Delta (denoted PRD), the Sichuan Basin (denoted SCH) and the Hubei–Hunan area (denoted HUZ), as shown in Fig. 1.
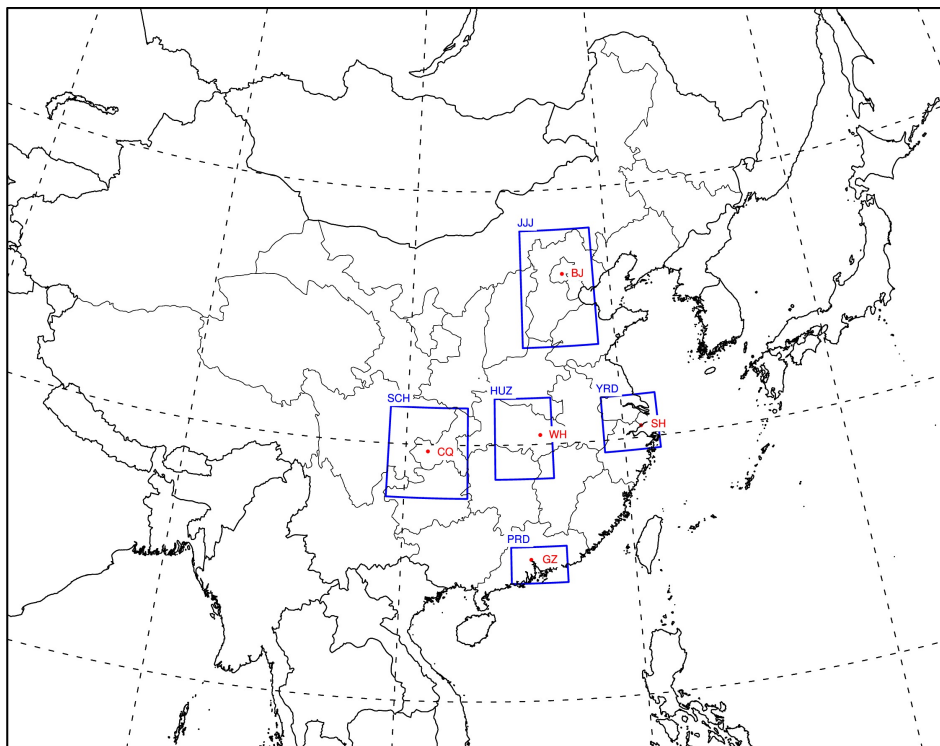
Figure 1. Simulation domain and locations of five selected regions in China. Note: JJJ: Jing-Jin-Ji area; YRD: Yangzi River Delta area; PRD: Pearl River Delta area; SCH: Sichuan Basin area; HUZ: Hubei–Hunan area.

2.2 Simulation design

Table 1 summarizes the scenario design in this study. In the baseline simulation (denoted SimBL), no aerosol feedbacks either on photolysis rates or radiation were taken into account. In simulation SimNF, only aerosol feedbacks on photolysis rates were considered by embedding an inline photolysis calculation in the model which accounted for the modulation of photolysis due to ADEs. Finally, in simulation SimSF aerosol feedbacks were considered on both photolysis rates and radiation calculations. Differences between the simulations of SimNF and SimBL are considered as ADE impacts on O_3 through photolysis (denoted ΔPhotolysis). Similarly, differences between the simulations of SimSF and SimNF are considered as the ADE impacts on O_3 through dynamics (denoted ΔDynamics), and differences between the simulations of SimSF and SimBL represent the combined ADE impacts on O_3 due to both photolysis and dynamics (denoted ΔTotal).

2.3 Process analysis

In this study the PA methodology is used in the WRF-CMAQ model to analyze processes impacting simulated O_3 level. The integrated process rates (IPRs) track hourly contributions to O_3 from seven major modeled atmospheric processes that act as sinks or sources of O_3. These processes are gas-phase chemistry (denoted CHEM), cloud processes (i.e., the net effect of aqueous-phase chemistry, below- and in-cloud scavenging, and wet deposition, together denoted CLDS, dry deposition (denoted DDEP), horizontal advection (denoted HADV), horizontal diffusion (denoted HDIF), vertical advection (denoted ZADV) and turbulent mixing (denoted VDIF). The difference in IPRs among SimBL, SimNF and SimSF represents the response of individual process to ADEs. To enable the consistent examination of changes in the process due the ADEs across all concentration ranges, we examine changes in the IPRs normalized by the O_3 concentrations. The differences in these process rates (expressed in units h^{-1}) between the SimBL, SimSF and SimNF then provide estimates of the changes in process rates resulting from ADEs and are shown in the column (b) of Figs. 4 and 6 and (b)–(d) of Fig. 5.

Integrated reaction rates (IRRs) are used to investigate the relative importance of various gas-phase reactions in O_3 formation. Following the grouping approach of previous studies (Zhang et al., 2009; Liu et al., 2010; Xing et al., 2011), the chemical production of total odd oxygen (O_x) and the chain length of hydroxyl radical (OH) are calculated. Additionally, the ratio of the chemical production rate of H_2O_2 to that of HNO_3 ($P_{H_2O_2}/P_{HNO_3}$) is an estimated indicator of NO_x- or VOC- limited conditions for O_3 chemistry.

Table 1. Description of sensitivity simulations in this study.

Short name	Simulation description	Aerosol impacts on photolysis calculations	Aerosol impacts on radiation calculations
SimBL	Baseline simulation	No	No
SimNF	No aerosol feedback simulation	Yes	No
SimSF	Aerosol feedback simulation	Yes	Yes

3 Results

3.1 O$_3$ response to ADEs

The simulated surface DM1O$_3$ in SimBL, SimNF and SimSF is compared in Fig. 2a–c. In January, higher DM1O$_3$ concentrations are seen in PRD, where solar radiation is stronger than in the north. The model generally captured the spatial pattern with highest DM1O$_3$ in PRD over the simulated domain. Simulated DM1O$_3$ in YRD, SCH and HUZ is higher than observations. Such overestimation might be associated with the relatively coarse spatial resolution in the model. NO titration effects in urban areas were not well represented in the model. In July, high DM1O$_3$ areas are located towards the north, especially in the JJJ and YRD regions, which have relatively larger NO$_x$ and VOC emission density and favorable meteorological conditions (e.g., less rain and moderate solar radiation).

In January, O$_3$ production in north China is occurs in a VOC-limited regime (e.g., Liu et al., 2010); thus, increases in NO$_x$ at the surface stemming from the stabilized atmosphere by ADEs (Jacobson et al., 2007; Mathur et al., 2010; Ding et al., 2013; Xing et al., 2015) inhibit O$_3$ formation due to enhanced titration by NO. As seen in Fig. 2d, the ΔDynamics reduced DM1O$_3$ in eastern China by up to 24 µg m^{-3} but slightly increased DM1O$_3$ in parts of southern China by up to 7 µg m^{-3}. The decrease in incoming solar radiation due to ADEs significantly reduces the photolysis rates in east China. As seen in Fig. 2e, the ΔPhotolysis reduced DM1O$_3$ domain-wide by up to 16 µg m^{-3}. The combined effect of both ΔDynamics and ΔPhotolysis results in an overall reduction in DM1O$_3$ as evident across the JJJ and SCH regions with monthly-average reductions of up to 39 µg m^{-3}.

In July, the O$_3$ chemistry changes from a VOC-limited to an NO$_x$-limited regime across most of China. Therefore, an increase in NO$_x$ concentration due to the stabilization of the atmosphere associated with the ADEs, facilitates O$_3$ formation. The ΔDynamics increased DM1O$_3$ across most areas of China, particularly in JJJ, YRD and SCH by up to 5 µg m^{-3}, with the exception of the PRD region where DM1O$_3$ decreased. The ΔPhotolysis results in contrasting impacts in July compared to January, as it increased DM1O$_3$ in most polluted areas including JJJ, YRD, PRD, HUZ, although the solar radiances were reduced due to ΔPhotolysis. This behavior is likely due to enhanced aerosol scattering associated

with higher summertime SO$_4^{2-}$ levels (He and Carmichael, 1999; Jacobson, 1998). Similar results were found in Tie et al. (2005), who reported that surface-layer photolysis rates in eastern China were reduced less significantly in summer than in winter. The resultant enhancements in photolysis rates can then cause the noted higher concentrations. More importantly, the diurnal analysis (discussed in the next section) suggested that the reduced photolysis during the early morning in SimNF enhances the ambient precursor concentrations (due to less reaction in the early morning) at noon when O$_3$ reaches the daily maximum. This increase in precursor concentrations then leads to enhanced O$_3$ formation later in the day which compensates for or even outweighs the disbenefit from the reduced solar radiances. In summer, ΔDynamics results in a much stronger influence on DM1O$_3$ than ΔPhotolysis, and the combined impact of ADEs increased O$_3$ in most of regions in China by up to 4 µg m^{-3}.

The impact of the ADEs on O$_3$ is further explored by examining the relationship between the observed and simulated O$_3$ concentrations (DM1O$_3$, daily values of the cities located in China) as a function of the observed PM$_{2.5}$ concentrations (observed daily averaged values in those cities), as displayed in Fig. 3. The predicted ozone concentrations under both low and high PM$_{2.5}$ levels are compared in Table 2. In regards to model performance for DM1O$_3$ simulations, the model generally exhibits a slight high bias in January but a low bias in July across the five regions. The inclusion of ADEs moderately reduced O$_3$ concentrations in January and slightly increased O$_3$ in July, resulting in a reduction in bias and improved performance for DM1O$_3$ simulation in both January and July for most of the regions. Comparing the O$_3$ responses to ADEs (see Δ-ADE in Table 2) under low and high PM$_{2.5}$ levels reveals that the O$_3$ responses to ADEs are larger under high PM$_{2.5}$ levels, indicating the positive correlations between O$_3$ responses and PM$_{2.5}$ levels.

Interestingly, from low to moderate PM$_{2.5}$ levels (i.e., PM$_{2.5}$ < 120 µg m^{-3}), higher O$_3$ concentration occur with higher PM$_{2.5}$ concentrations, which is evident in both observations and simulations, suggestive of common precursors (e.g., NO$_x$), source sectors and/or transport pathways contributing to both O$_3$ and PM$_{2.5}$ in these regions. However, a negative correlation between O$_3$ and PM$_{2.5}$ is evident in winter when PM$_{2.5}$ can reach high levels larger than 120 µg m^{-3}, indicating the strong ADE impacts on O$_3$ through both feed-
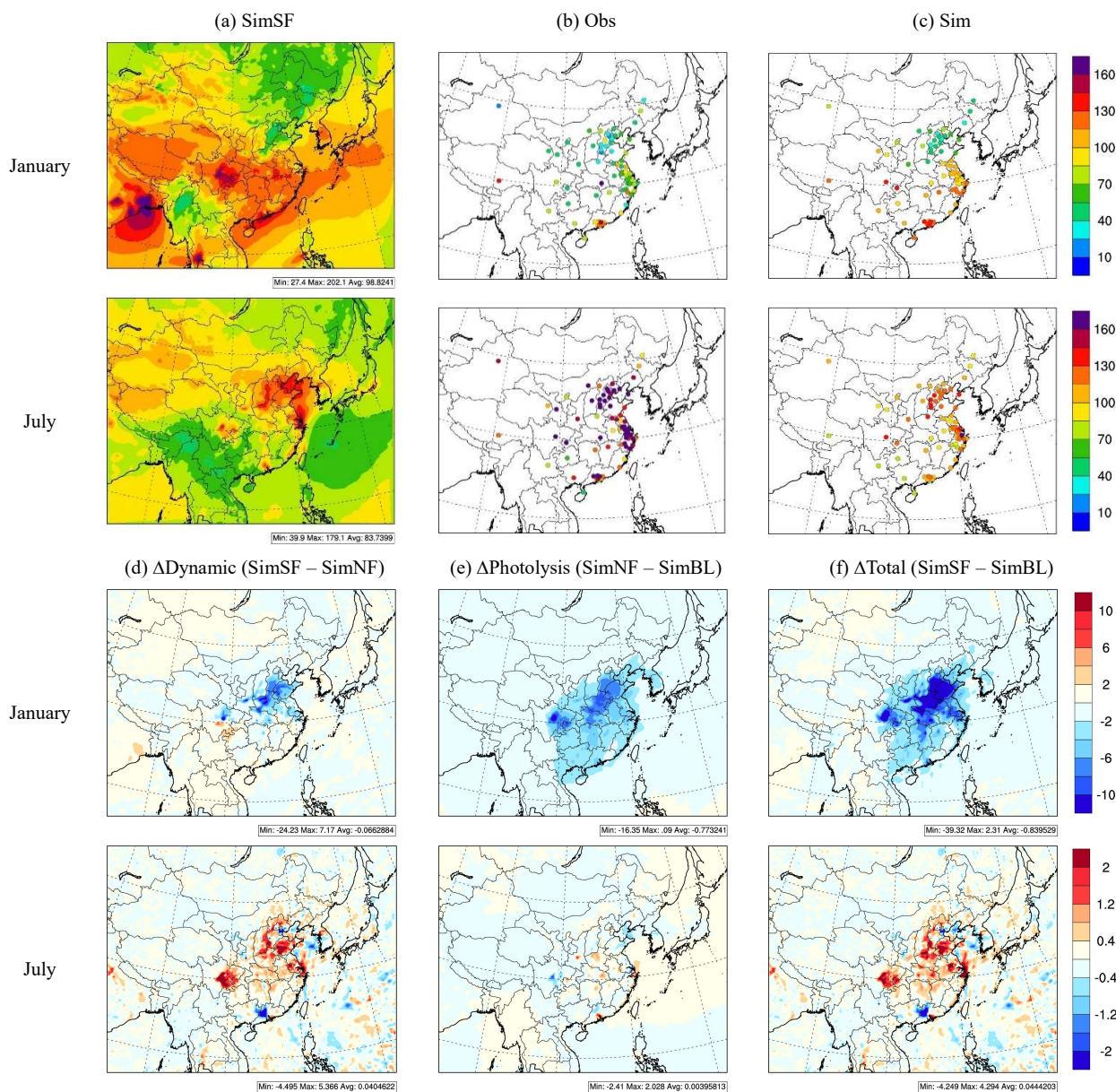
Figure 2. Observed and simulated O_3 and its response to ADEs (monthly average of daily 1 h maxima, $\mu g\,m^{-3}$).

backs to dynamics and photolysis which significantly reduced O_3.

3.2 IPRs response to ADEs

To further explore the ADE impacts on simulated O_3, the integrated process contributions are further analyzed in three ways: (a) 24 h diurnal variations in process contributions to simulated surface O_3 (Fig. 4); (b) vertical profiles from ground up to 1357 m a.g.l. (above ground level, in model layers 1–10) at noon (Fig. 5); and (c) correlations with near-ground $PM_{2.5}$ (average concentrations between the ground and 355 m a.g.l.; model layers 1–5) (Fig. 6). In the following,

we limit our discussion to the analysis of model results for the JJJ region, which exhibited the strongest ADEs among the regions; similar results were found for the other four regions and can be found in the Supplement.

Diurnal variation in process contributions from chemistry (CHEM), dry deposition (DDEP) and vertical turbulent mixing (VDIF), which together contribute to more than 90 % of the O_3 rate of change for the JJJ region, are illustrated in Fig. 4. The diurnal variation in IPRs for other processes and their response to ADEs are displayed in Fig. S1 in the Supplement for JJJ and Figs. S2–S5 for the other four regions.

Table 2. Comparison of model performance in ozone prediction across three simulations (monthly average of daily 1 h maxima).

	Region	OBS	Normalized mean bias			Δ-ADE*	OBS	Normalized mean bias			Δ-ADE
			SimSF	SimNF	SimBL			SimSF	SimNF	SimBL	
		Low PM$_{2.5}$ (< 60 µg m^{-3})					High PM$_{2.5}$ (< 60 µg m^{-3})				
		(μg m^{-3})				(μg m^{-3})	(μg m^{-3})				(μg m^{-3})
January	JJJ	62.52	3 %	4 %	5 %	−1.05	37.02	22 %	36 %	53 %	−11.36
	YRD	63.89	38 %	41 %	43 %	−2.76	66.74	54 %	59 %	67 %	−8.85
	PRD	97.25	25 %	26 %	29 %	−4.52	122.61	6 %	5 %	9 %	−4.63
	HUZ	47.67	172 %	173 %	193 %	−10.17	67.29	107 %	125 %	142 %	−23.9
	SCH	88.63	−43 %	−40 %	−38 %	−3.85	111.19	−5 %	2 %	8 %	−13.78
	China	76.61	30 %	31 %	34 %	−2.96	62.68	42 %	48 %	56 %	−8.61
July	JJJ	159.27	−29 %	−28 %	−28 %	−0.51	178.54	−25 %	−25 %	−25 %	1.02
	YRD	171.04	−31 %	−31 %	−32 %	0.84	233.13	−24 %	−25 %	−23 %	−0.51
	PRD	129.02	−20 %	−19 %	−20 %	−0.09	312.21	−44 %	−45 %	−46 %	4.92
	HUZ	187.44	−36 %	−37 %	−37 %	1.39	208.99	−27 %	−28 %	−29 %	4.19
	SCH	163.81	−38 %	−38 %	−39 %	0.77	191.19	−30 %	−31 %	−31 %	1.18
	China	145.24	−28 %	−28 %	−28 %	0.3	181.65	−25 %	−25 %	−25 %	0.9

* Δ-ADE represents the O$_3$ response to ADEs, which is calculated from the difference between SimSF and SimBL.
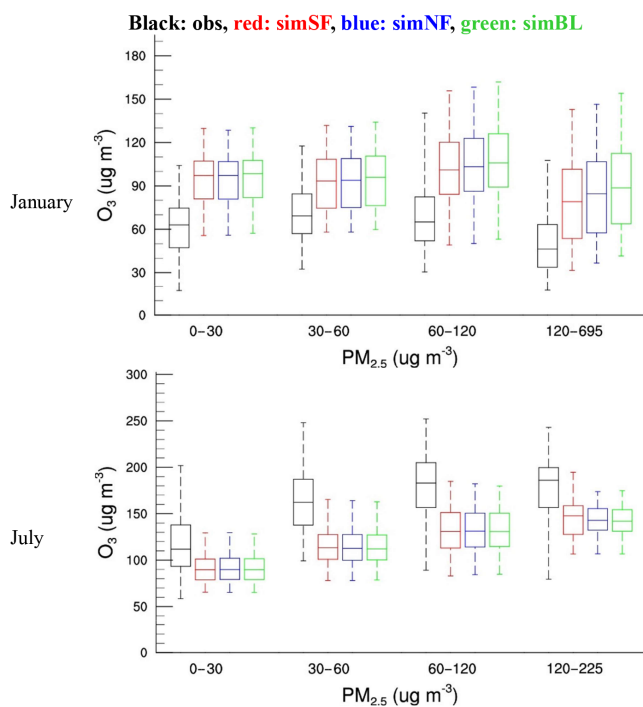

Figure 3. Observed and simulated surface O$_3$ concentration against PM$_{2.5}$ concentration (O$_3$ is daily 1 h maximum of monitoring sites over China – unit: µg m^{-3}; PM$_{2.5}$ is the daily average of those site – unit: µg m^{-3}).

For surface-level O$_3$, VDIF is the major source and DDEP is the major sink (Fig. S1). The stabilization of the atmosphere due to ΔDynamics leads to lower dry deposition rates (due to lower dry deposition velocity from the enhanced aerodynamic resistance) and thus increases surface O$_3$. The largest impact of ΔDynamics on DDEP occurs during early morning and late afternoon, which is consistent with the response of the PBL height to ADEs noted in our previous analysis (Xing et al., 2015a).

As expected, CHEM is the second-largest sink for surface O$_3$ during January but a source of surface O$_3$ during the daytime in July. The ΔDynamics increased the surface O$_3$ around noon in both January and July for almost all regions (no impacts in PRD and YRD in January; see Figs. S2–S3), since increased stability due to ΔDynamics concentrated more precursors locally, leading to enhanced O$_3$ formation during the photochemically most active period of the day. The ΔDynamics reduced the surface O$_3$ around late afternoon in January in all regions. This is because the increased atmospheric stability during late afternoon and evening hours increased NO$_x$ concentration, which titrated more O$_3$. The ΔPhotolysis reduced surface O$_3$ in all regions in January. These reductions were more pronounced during the early morning hours when the photolysis rate are most sensitive to the radiation intensity. The ΔPhotolysis resulted in comparatively larger reductions in surface O$_3$ during the early morning and late afternoon hours in July but slightly increased surface O$_3$ at noon for most of the regions. This increase in O$_3$ can be hypothesized to result from the following sequence of events. Slower photochemical reaction in the morning in the ΔPhotolysis case leads to higher levels of precursors, whose accumulation then enhances O$_3$ formation at noon. This hypothesis is further confirmed by the changes in the diurnal variation in NO$_2$, which suggest that higher NO to NO$_2$ conversion during early morning results in enhanced daytime NO$_2$ levels (see Fig. S6), consequently leading to higher noontime O$_3$.
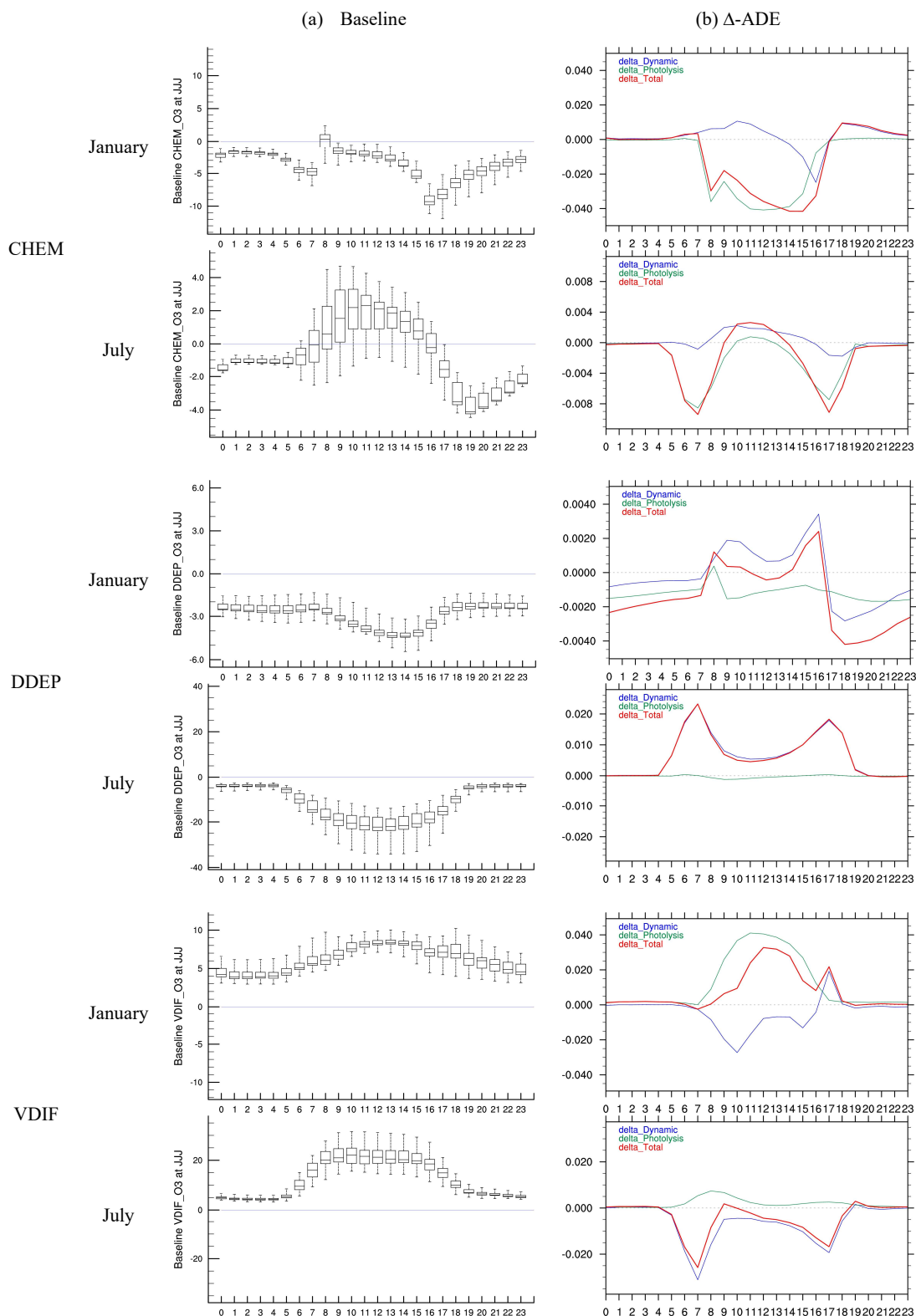
Figure 4. Diurnal variation in selected integrated process contributions to surface O_3 concentration in JJJ. The calculation is based on the average of grid cells in JJJ; **(a)** baseline is the simulated O_3 in SimBL (unit: ppb h^{-1}); **(b)** Δ-ADE is the difference in normalized IPRs between simulations (unit: h^{-1}). Delta_Dynamic is the difference between SimSF and SimNF; delta_Photolysis is the difference between SimNF and SimBL; delta_Total is the difference between SimSF and SimBL).
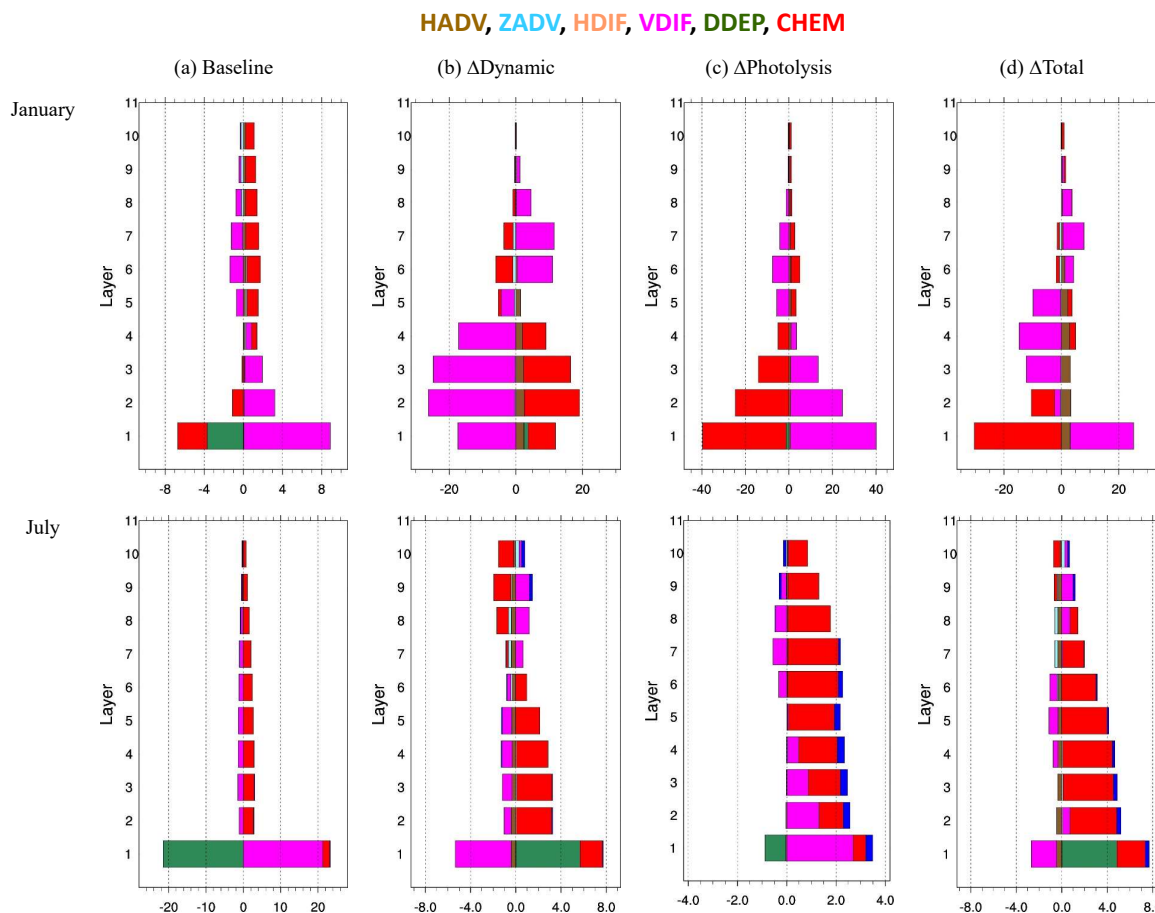
HADV, ZADV, HDIF, VDIF, DDEP, CHEM

Figure 5. Vertical profile of integrated process contributions to surface O$_3$ concentration at noon in JJJ. Full-layer heights above ground are 40, 96, 160, 241, 355, 503, 688, 884, 1100 and 1357 m; **(a)** baseline is the simulated O$_3$ in SimBL (unit: ppb h^{-1}); **(b)** ΔDynamic is the difference in normalized IPRs between SimSF and SimNF (unit: h^{-1}); **(c)** ΔPhotolysis is the difference in normalized IPRs between SimNF and SimBL (unit: h^{-1}); **(d)** ΔTotal is the difference in normalized IPRs between SimSF and SimBL (unit: h^{-1}).

For O$_3$ aloft (from 100 to 1600 m above ground), as seen in Fig. 5, CHEM is the major source of O$_3$ at noon both in January and in July. The ΔDynamics increased near-surface O$_3$ (below 500 m; model layers 1–6) but reduced upper-level O$_3$ (above 500 m; model layers 7–10) because increased stability of the atmosphere concentrated precursor emissions within a shallower layer resulting in higher O$_3$ production. The ΔPhotolysis case considerably reduced near-surface O$_3$ at noon in January. In July, ΔPhotolysis increased upper-level O$_3$ at noon. Higher levels of precursors at noon might be the reason for such enhancement (see Fig. S6).

The daytime near-ground-averaged (between the ground and 350 m a.g.l.; layers 1–5) IPR responses to ADEs are shown in Fig. 6 for JJJ and in Fig. S7 for other regions. The IPR and its responses are presented as a function of near-ground-averaged PM$_{2.5}$ concentrations. As shown in Fig. 6, as PM$_{2.5}$ concentrations increase, the positive contribution of CHEM in July becomes larger, while the negative contribution of CHEM in January becomes smaller. The overall

ADEs enhanced CHEM and thus increased O$_3$ concentration in July, and such enhancement is generally larger for higher PM$_{2.5}$ loading. In contrast, in January overall ADEs resulted in higher rates of O$_3$ destruction due to chemistry (negative contribution of CHEM), and the magnitude of this sink increased as PM$_{2.5}$ concentrations increase. The reduction of O$_3$ stemming from the enhancements in the chemical sinks is the dominant impact of ADEs in January. The enhanced positive contribution of CHEM due to ΔDynamics was partially compensated for by the reduction from ΔPhotolysis (see Fig. S7), resulting in a slight increase in the positive CHEM contribution to O$_3$ in July.

DDEP is the major sink of daytime O$_3$ during both January and July. The increased stability due to ADEs reduced deposition velocity and thus increased O$_3$. These effects become larger with increasing PM$_{2.5}$ concentrations. Thus, weaker removal of O$_3$ from DDEP associated with ADEs contributed to higher O$_3$ in most regions during both January and July.
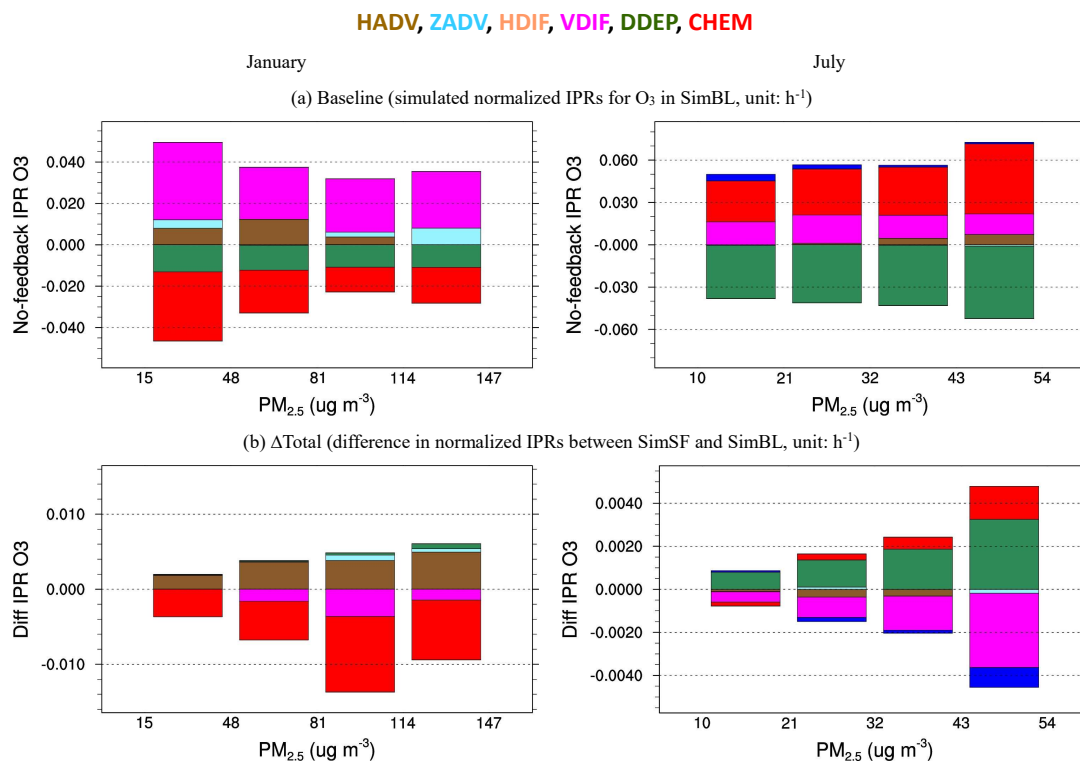
Figure 6. Integrated process contributions to daytime near-ground-level O_3 under different $PM_{2.5}$ levels in JJJ (between the ground and 350 m a.g.l.; model layers 1–5).

An enhanced O_3 source of CHEM and reduced O_3 sink of DDEP is the dominant impact of ADEs in July.

3.3 IRR response to ADEs

The simulated midday average (11:00–13:00 local time) surface O_x (defined as the sum of O, O_3, NO_2, NO_3, N_2O_5, HNO_3, peroxynitric acid, alkyl nitrates and peroxyacyl nitrates) and OH and their responses to ADEs is shown in Fig. 7. Both O_x and OH are significantly reduced in the ΔPhotolysis case in January throughout the modeling domain. Both O_x and OH also show reductions in the middle portions of east China in the ΔDynamics case in January. Together, the combined ADE impacts result in reduced O_x and OH in January, with widespread reductions primarily due to ADEs on photolysis. In July, ΔPhotolysis increased midday OH across most of China (Fig. 7), which is consistent with the increase in O_3 at noon stemming from a higher level of precursor accumulation due to ΔPhotolysis. The overall ADE impact on OH is controlled by ΔPhotolysis and results in increased midday OH across most of China. For O_x, however, the impact of ΔDynamics outweighs the impact from ΔPhotolysis, resulting in increase in O_x concentrations in east China including YRD, SCH and HUZ.

To further examine the response of O_x to ADEs, in Fig. 8 we examine vertical profiles of the integrated reaction rates

at noon for the JJJ region. The stabilization of the atmosphere due to ΔDynamics concentrates precursors within a lower PBL, resulting in an increased total O_x production rate (P_{totalO_x}) mostly in near-ground model layers (below 500 m; model layers 1–6); in magnitude aloft (above 500 m; model layers 7–10), this change in P_{totalO_x} is smaller in January and becomes decreasing in July. The reduction of P_{totalO_x} due to ΔPhotolysis is greatest at the surface in January and declines with altitude and even becomes reversed at high layers (about 1300 m; model layer 10) (Fig. 8a). The overall ADE impact in January is mainly dominated by ΔPhotolysis, which largely outweighs the impact of ΔDynamics (Fig. 8a). However, in July (Fig. 8b), ΔPhotolysis enhanced P_{totalO_x} across all layers. The P_{totalO_x} shows small decreases at high altitudes but a significant increase in near-ground model layers (below 500 m; model layers 1–6) due to the combined ADEs in July.

The changes in vertical profiles of production rates of new OH (P_{NewOH}) and reacted OH ($P_{ReactedOH}$) are similar to those of P_{totalO_x}, with the noted decreases in January dominated by ΔPhotolysis. In contrast, the increases in July result from contributions from both ΔPhotolysis and ΔDynamics.

An analysis of the chain length is important to understand the characteristics of chain reaction mechanisms. The OH chain length (denoted OH_CL) is determined by the ratio of $P_{ReactedOH}$ to P_{NewOH}. ΔDynamics concentrated more
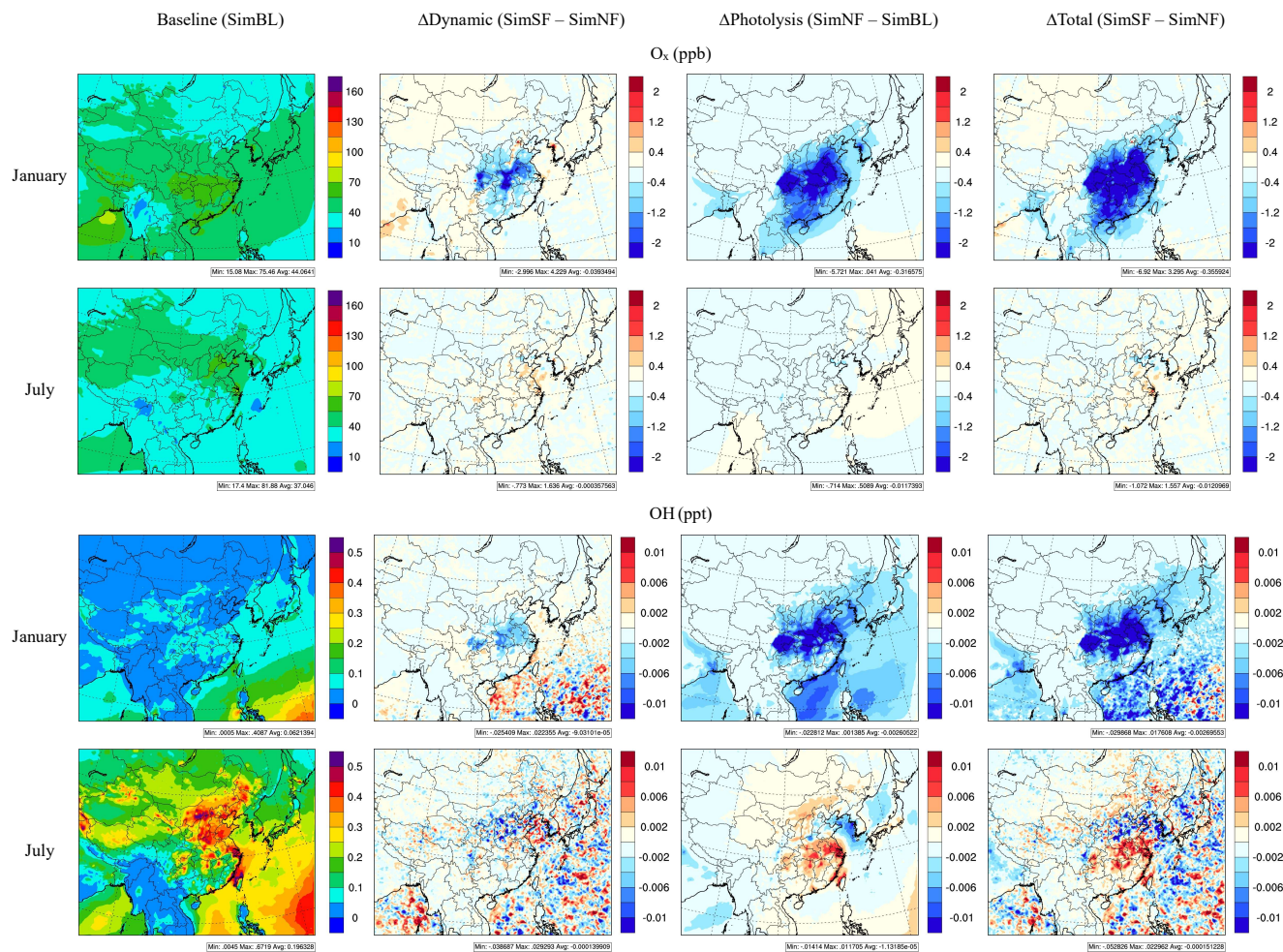
Figure 7. Impacts of ADEs on surface O_x and OH (monthly average of noon time 11:00–13:00 local time).

NO_x at the surface, thus leading to an increased OH_CL (i.e., more reacted OH than new OH) in the near-ground layers but a decreased OH_CL in the upper layers. In January, the ΔPhotolysis reduced P_{NewOH} more than $P_{ReactedOH}$ (probably because of more abundance of NO_x resulting from photolysis attenuation and consequently reduced photochemistry), thereby leading to an increased OH_CL. In July, ΔPhotolysis enhanced both P_{NewOH} and $P_{ReactedOH}$, particularly in the upper layers. The OH_CL is increased by ΔPhotolysis because higher NO_x levels (see Fig. S6) cause more OH to be reacted. Thus the surface OH_CL at noon is increased in both January and July from combined ADEs of ΔPhotolysis and ΔDynamics, indicating a stronger propagation efficiency of the chain.

The production rates of H_2O_2 ($P_{H_2O_2}$) and HNO_3 (P_{HNO_3}) and their responses to ADEs are also summarized in Fig. 8 (average for midday hours) for the JJJ region (similar illustrations for the other regions can be found in the supplemental Figs. S8–S11. Smaller ratios of $P_{H_2O_2}/P_{HNO_3}$ are noted in January compared to July, indicating a stronger VOC-limited

regime in January for all regions. The ΔDynamics increases P_{HNO_3} but decreases $P_{H_2O_2}$ in both January and July because the enhanced NO_x at the surface in a more stable atmosphere likely shifts O_3 chemistry towards NO_x-rich conditions. The ΔPhotolysis reduced both $P_{H_2O_2}$ and P_{HNO_3}, but the ratio of $P_{H_2O_2}/P_{HNO_3}$ is decreased due to a larger reduction in $P_{H_2O_2}$ than P_{HNO_3}. The combined impacts of ΔDynamics and ΔPhotolysis result in a shift towards more VOC-limited conditions in the near-surface layers during both January and July.

4 Summary

The impacts of ADEs on tropospheric ozone were quantified by using the two-way coupled meteorology and atmospheric chemistry WRF-CMAQ model using a process analysis methodology. Two manifestations of ADE impacts on O_3 – changes in atmospheric dynamics (ΔDynamics) and changes in photolysis rates (ΔPhotolysis) – were systematically evaluated through simulations that isolated their
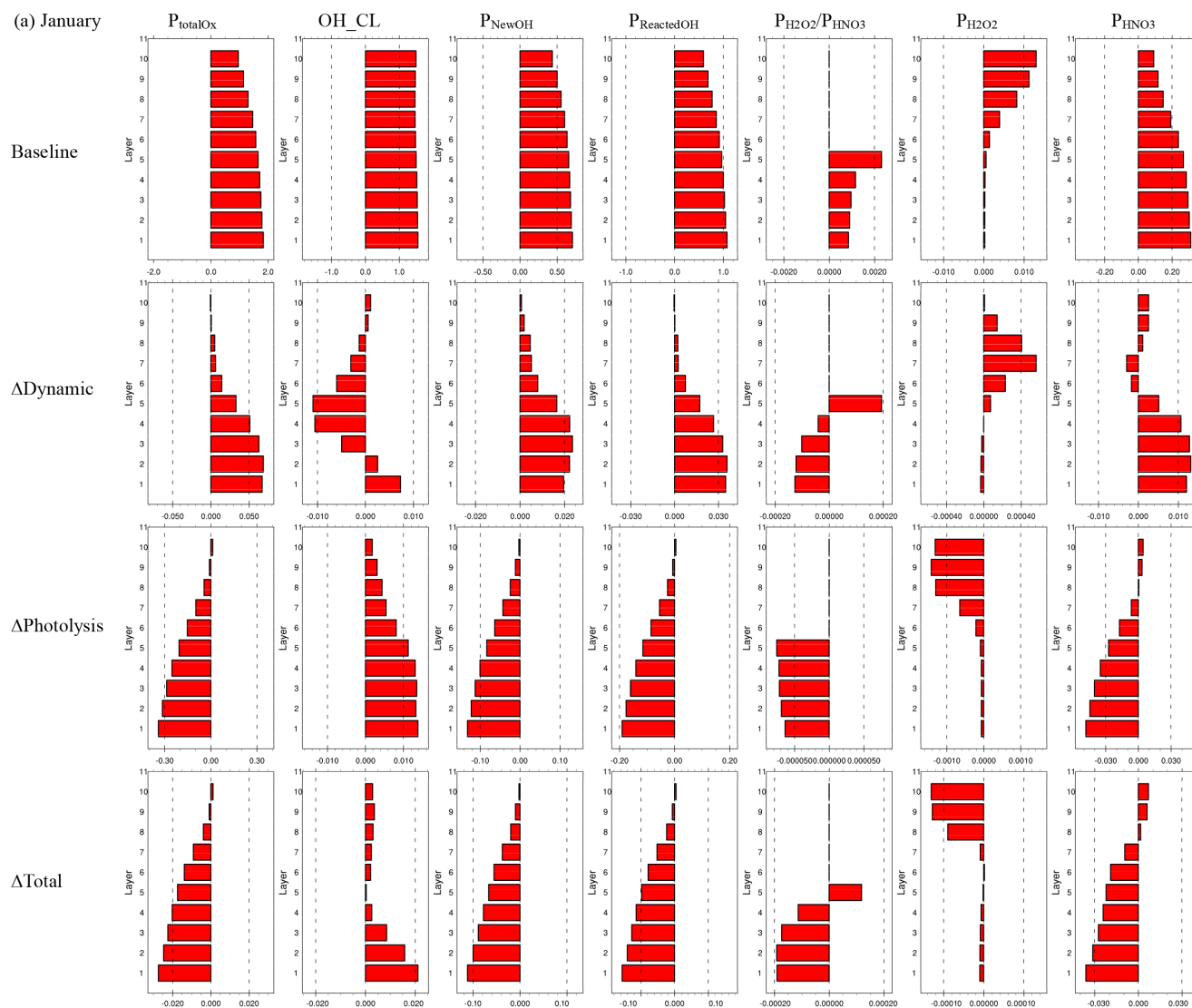
Figure 8.

impacts on modeled process rates over China for winter and summer conditions (represented by the months of January and July in 2013, respectively). Results suggest that the model performance for surface DM1O$_3$ simulations improved after the inclusion of ADEs, which moderately reduced the high bias in January and low bias in July. In winter, the inclusion of ADE impacts resulted in an overall reduction in surface DM1O$_3$ across China by up to $39\,\mu g\,m^{-3}$. Changes both in photolysis and atmospheric dynamics due to ADEs contributed to the reductions in DM1O$_3$ in winter. In contrast during July, the impact of ADEs increased surface DM1O$_3$ across China by up to $4\,\mu g\,m^{-3}$. The summertime increase in DM1O$_3$ results primarily from ADE-induced effects on atmospheric dynamics. It can thus be postulated that reducing ADEs will have the potential risk of increasing O$_3$

in winter but will benefit the reduction in maximum O$_3$ in summer.

Results from IPR analysis suggest that the ADE impacts exhibit strong vertical and diurnal variations. The ADE-induced decrease in modeled DM1O$_3$ in January primarily results from ΔPhotolysis, which reduced the chemical production of O$_3$ in the near-ground layers. The increase in DM1O$_3$ in July due to ADEs results from a weaker dry deposition sink as well as a stronger chemical source due to higher precursor concentrations in a more stable and shallow PBL. These impacts become stronger under higher PM$_{2.5}$ concentrations when ADEs are larger.

The combined ADE impacts reduce O$_x$ in January due to ΔPhotolysis but slightly increase O$_x$ in July due to ΔDynamics. OH is reduced by ADEs in January. However, midday OH concentrations during summertime
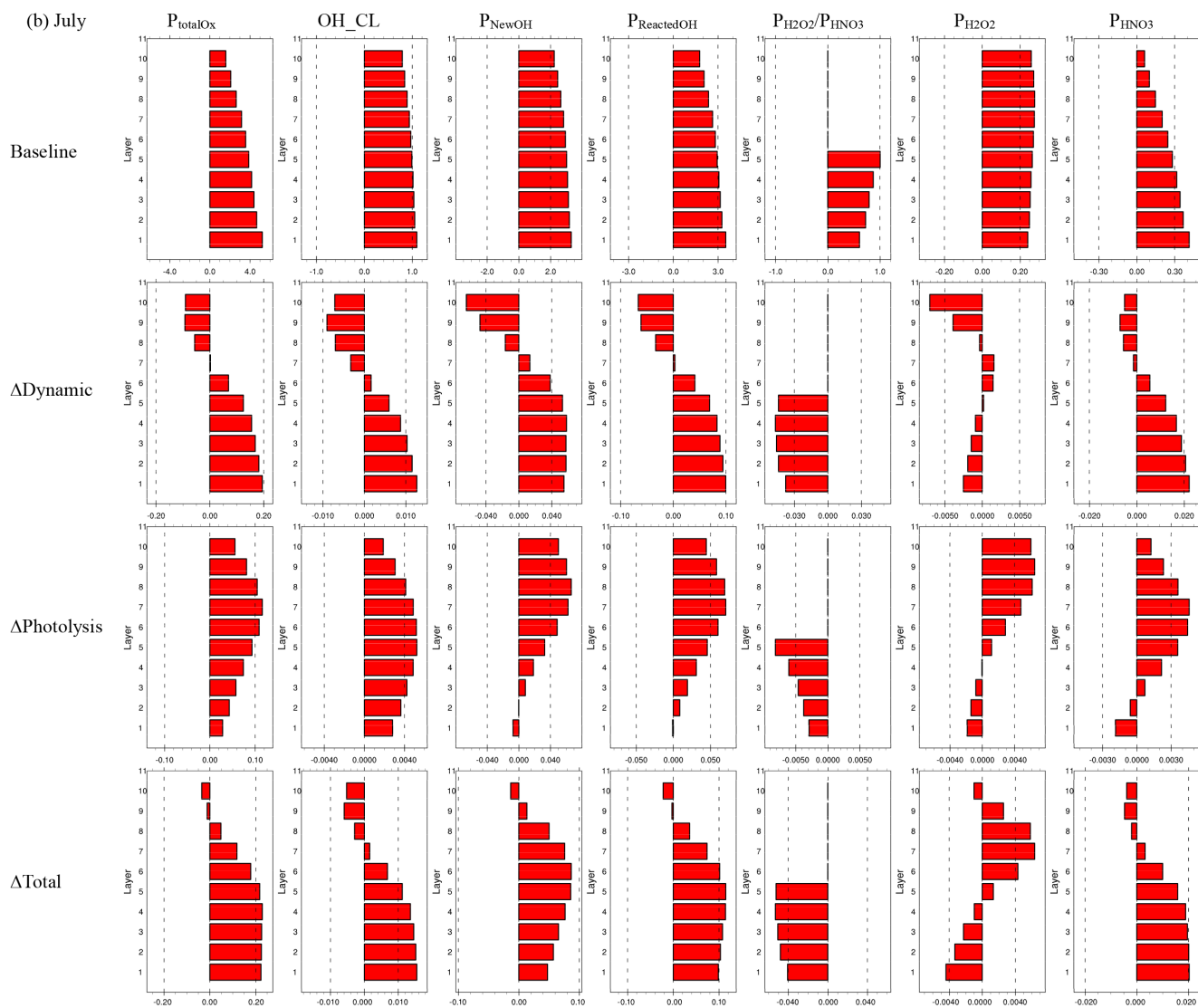
Figure 8. Vertical profile of integrated reaction rates in JJJ at noon. Full-layer heights above ground are 40, 96, 160, 241, 355, 503, 688, 884, 1100 and 1357 m; baseline is the simulation in SimBL; ΔDynamic is the difference between SimSF and SimNF; ΔPhotolysis is the difference between SimNF and SimBL; ΔTotal is the difference between SimSF and SimBL; P_{totalO_x} is total O_x production rate (unit: ppb h^{-1}); OH_CL is OH chain length; P_{NewOH} is the production rate of new OH (unit: ppb h^{-1}); $P_{ReactedOH}$ is the production rate of reacted OH (unit: ppb h^{-1}); $P_{H_2O_2}$ is the production rate of H$_2$O$_2$ (unit: ppb h^{-1}); P_{HNO_3} is the production rate of HNO$_3$ (unit: ppb h^{-1}); the ratio of $P_{H_2O_2}/P_{HNO_3}$ is only shown for layers 1–5.

show enhancements associated with both ΔPhotolysis and ΔDynamics, indicating a stronger midday atmospheric oxidizing capacity in July. An increased OH chain length in the near-ground layers is modeled both in January and July, indicating a stronger propagation efficiency of the chain reaction. In both January and July, P_{HNO_3} is increased and $P_{H_2O_2}$ is decreased due to ΔDynamics, and both are reduced due to ΔPhotolysis. The ratio of $P_{H_2O_2}/P_{HNO_3}$ is decreased due to the combined impacts of ΔDynamics and ΔPhotolysis, indicating a shift towards more VOC-limited conditions due

to ADEs in the near-ground layers during both January and July.

Thus aerosol direct effects on both photolysis rates as well as atmospheric dynamics can impact O$_3$ formation rates and its local and regional distributions. Comparisons of integrated process rates suggest that the decrease in DM1O$_3$ in January results from a larger net chemical sink due to ΔPhotolysis, while the increase in DM1O$_3$ in July is mostly associated with the slower removal due to reduced deposition velocity as well as a stronger photochemistry due to ΔDynamics. The IRR analyses confirm that the process

contributions from chemistry to $DM1O_3$ can be influenced by both ΔDynamics and ΔPhotolysis. Reduced ventilation associated with ΔDynamics enhances the precursor levels, which increase the chemical production rate of O_x and OH, resulting in greater O_3 chemical formation at noon during both January and July. One the other hand, reduced photolysis rates in ΔPhotolysis result in lower O_3 in January. However, in July lower photolysis rates result in the accumulation of precursors during the morning hours, which eventually lead to higher O_3 production at noon.

The comparison of integrated reaction rates from the various simulations also suggest that the increased OH_CL and the shift towards more VOC-limited conditions are mostly associated with the higher NO_2 levels due to ADEs. This further emphasizes the importance of NO_x controls in air pollution mitigation. Traditionally, the co-benefits from NO_x control for ozone and PM reduction are mostly because NO_x is a common precursor for both O_3 and $PM_{2.5}$. This study suggests that effective controls on NO_x will not only gain direct benefits for O_3 reduction but can also indirectly reduce peak O_3 through weakening the ADEs from the reduced $PM_{2.5}$, highlighting co-benefits from NO_x controls for achieving both O_3 and $PM_{2.5}$ reductions.

Reducing aerosols will have substantial impacts on ozone. The quantification of the aerosol influence on ozone is important to understand co-benefits associated with reductions in both particulate matter and ozone. This study focused on the evaluation of ADE impacts, which were not well quantified previously. However, the heterogeneous reactions associated with aerosols, as well as the impacts of emission controls of gaseous precursors on both aerosols and ozone also need to be studied in order to fully understand the influence of reducing aerosols on ambient ozone.

Data availability. The observations from 74 cities across China used in this study is available from the China National Urban Air Quality Real-time Publishing Platform (http://113.108.142.147:20035/emcpublish/). Model outputs are available upon request from the corresponding author.

The Supplement related to this article is available online at https://doi.org/10.5194/acp-17-9869-2017-supplement.

Competing interests. The authors declare that they have no conflict of interest.

Disclaimer. Although this work has been reviewed and approved for publication by the U.S. Environmental Protection Agency, it does not necessarily reflect the views and policies of the agency.

References

Albrecht, B. A.: Aerosols, Cloud Microphysics, and Fractional Cloudiness, Science, 245, 1227–1230, 1989.

Anger, A., Dessens, O., Xi, F., Barker, T., and Wu, R.: China's air pollution reduction efforts may result in an increase in surface ozone levels in highly polluted areas, Ambio, 45, 254–265, 2016.

Appel, K. W., Pouliot, G. A., Simon, H., Sarwar, G., Pye, H. O. T., Napelenok, S. L., Akhtar, F., and Roselle, S. J.: Evaluation of dust and trace metal estimates from the Community Multiscale Air Quality (CMAQ) model version 5.0, Geosci. Model Dev., 6, 883–899, https://doi.org/10.5194/gmd-6-883-2013, 2013.

Benas, N., Mourtzanou, E., Kouvarakis, G., Bais, A., Mihalopoulos, N., and Vardavas, I.: Surface ozone photolysis rate trends in the Eastern Mediterranean: Modeling the effects of aerosols and total column ozone based on Terra MODIS data, Atmos. Environ., 74, 1–9, 2013.

Bian, H., Han, S., Tie, X., Sun, M., and Liu, A.: Evidence of impact of aerosols on surface ozone concentration in Tianjin, China, Atmos. Environ., 41, 4672–4681, 2007.

Bohren, C. F. and Huffman, D. R.: Absorption and Scattering of Light by Small Particles, Wiley-Interscience, New York, 530 pp., 1983.

Davis, J. M., Bhave, P. V., and Foley, K. M.: Parameterization of N_2O_5 reaction probabilities on the surface of particles containing ammonium, sulfate, and nitrate, Atmos. Chem. Phys., 8, 5295–5311, https://doi.org/10.5194/acp-8-5295-2008, 2008.

Dickerson, R. R., Kondragunta, S., Stenchikov, G., Civerolo, K. L., Doddridge, B. G., and Holben, B. N.: The impact of aerosols on solar ultraviolet radiation and photochemical smog, Science, 278, 827–830, 1997.

Ding, A. J., Huang, X., Nie, W., Sun, J. N., Kerminen, V. M., Petäjä, T., Su, H., Cheng, Y. F., Yang, X. Q., Wang, M. H., Chi, X. G., Wang, J. P., Virkkula, A., Guo, W. D., Yuan, J., Wang, S. Y., Zhang, R. J., Wu, Y. F., Song, Y., Zhu, T., Zilitinkevich, S., and Kulmala, M.: Black carbon enhances haze pollution in megacities in China, Geophys. Res. Lett., 43, 2873–2879, https://doi.org/10.1002/2016GL067745, 2016.

Gan, C. M., Hogrefe, C., Mathur, R., Pleim, J., Xing, J., Wong, D., Gilliam, R., Pouliot, G., and Wei, C.: Assessment of the aerosol optics component of the coupled WRF-CMAQ model using CARES field campaign data and s single column model, Atmos. Environ., 115, 670–682, 2015.

Haagen-Smit, A. J. and Fox, M. M.: Photochemical ozone formation with hydrocarbons and automobile exhaust, Air Repair, 4, 105–136, 1954.

Hansen, J., Sato, M., and Ruedy, R.: Radiative forcing and climate response, J. Geophys. Res.-Atmos., 102, 6831–6864, 1997.

He, S. and Carmichael, G. R.: Sensitivity of photolysis rates and ozone production in the troposphere to aerosol properties, J. Geophys. Res.-Atmos., 104, 26307–26324, 1999.

Hogrefe, C., Pouliot, G., Wong, D., Torian, A., Roselle, S., Pleim, J., and Mathur, R.: Annual application and evaluation of the on-line coupled WRF–CMAQ system over North America under AQMEII phase 2, Atmos. Environ., 115, 683–694, 2015.

Jacobson, M. Z.: Studying the effects of aerosols on vertical photolysis rate coefficient and temperature profiles over an urban airshed, J. Geophys. Res., 103, 10593–10604, 1998.

Jacobson, M. Z.: Control of fossil-fuel particulate black carbon plus organic matter, possibly the most effective method of slowing global warming, J. Geophys. Res., 107, 4410, https://doi.org/10.1029/2001JD001376, 2002.

Jacobson, M. Z.: Short-term effects of controlling fossil-fuel soot, biofuel soot and gases, and methane on climate, Arctic ice, and air pollution health, J. Geophys. Res., 115, D14209, https://doi.org/10.1029/2009JD013795, 2010.

Jacobson, M. Z., Kaufman, Y. J., and Rudich, Y.: Examining feedbacks of aerosols to urban climate with a model that treats 3-D clouds with aerosol inclusions, J. Geophys. Res., 112, D24205, https://doi.org/10.1029/2007JD008922, 2007.

Jang, J. C., Jeffries, H. E., and Tonnesen, S.: Sensitivity of ozone to model grid resolution-II. Detailed process analysis for ozone chemistry, Atmos. Environ., 29, 3101–3114, 1995.

Li, J., Wang, Z., Wang, X., Yamaji, K., Takigawa, M., Kanaya, Y., Pochanart, P., Liu, Y., Irie, H., Hu, B., and Tanimoto, H.: Impacts of aerosols on summertime tropospheric photolysis frequencies and photochemistry over Central Eastern China, Atmos. Environ., 45, 1817–1829, 2011.

Liao, H. and Seinfeld, J. H.: Global impacts of gas-phase chemistry–aerosol interactions on direct radiative forcing by anthropogenic aerosols and ozone, J. Geophys. Res., 110, D18208, https://doi.org/10.1029/2005JD005907, 2005.

Liou, K. and Ou, S.: The role of cloud microphysical processes in climate – an assessment from a one-dimensional perspective, J. Geophys. Res.-Atmos., 94, 8599–8607, 1989.

Liu, X. H., Zhang, Y., Xing, J., Zhang, Q., Wang, K., Streets, D. G., Jang, C., Wang, W. X., and Hao, J. M.: Understanding of regional air pollution over China using CMAQ, part II. Process analysis and sensitivity of ozone and particulate matter to precursor emissions, Atmos. Environ., 44, 3719–3727, 2010.

Lou, S. J., Liao, H., and Zhu, B.: Impacts of aerosols on surface-layer ozone concentrations in China through heterogeneous reactions and changes in photolysis rates, Atmos. Environ., 85, 123–138, 2014.

Mathur, R., Pleim, J., Wong, D., Otte, T. L., Gilliam, R. C., Roselle, S. J., Young, J. O., Binkowski, F. S., and Xiu, A.: The WRF-CMAQ Integrated On-Line Modeling System: Development, Testing, and Initial Applications, chap. 2, edited by: Douw, G. S. and Rao, S. T., Air Pollution Modeling and its Applications XX, Springer Netherlands, Netherlands, 155–159, 2010.

Mathur, R., Pleim, J., Wong, D., Hogrefe, C., Xing, J., Wei, C., Gan, C.-M., and Binkowski, F.: Investigation of Trends in Aerosol Direct Radiative Effects over North America Using a Coupled Meteorology-Chemistry Model, in: Air Pollution Modeling and its Application XXIII, Springer International Publishing, 67–72, 2014.

Mitchell, J. F. B., Davis, R. A., Ingram, W. J., and Senior, C. A.: On Surface Temperature, Greenhouse Gases, and Aerosols: Models and Observations, J. Climate, 8, 2364–2386, 1995.

Pleim, J., Young, J., Wong, D., Gilliam, R., Otte, T., and Mathur, R.: Two-Way Coupled Meteorology and Air Quality Modeling, Air Pollution Modeling and Its Application XIX, NATO Science for Peace and Security Series C, Environmental Security, 2, 235–242, 2008.

Pozzoli, L., Bey, I., Rast, S., Schultz, M. G., Stier, P., and Feichter, J.: Trace gas and aerosol interactions in the fully coupled model of aerosol-chemistry-climate ECHAM5-HAMMOZ: 1. Model description and insights from the spring 2001 TRACE-P experiment, J. Geophys. Res., 113, D07308, https://doi.org/10.1029/2007JD009007, 2008.

Sarwar, G., Luecken, D., Yarwood, G., Whitten, G. Z., and Carter, W. P.: Impact of an updated carbon bond mechanism on predictions from the CMAQ modeling system: Preliminary assessment, J. Appl. Meteorol. Clim., 47, 3–14, 2008.

Sarwar, G., Simon, H., Bhave, P., and Yarwood, G.: Examining the impact of heterogeneous nitryl chloride production on air quality across the United States, Atmos. Chem. Phys., 12, 6455–6473, https://doi.org/10.5194/acp-12-6455-2012, 2012.

Sarwar, G., Simon, H., Xing, J., and Mathur, R.: Importance of tropospheric $ClNO_2$ chemistry across the Northern Hemisphere, Geophys. Res. Lett., 41, 4050–4058, 2014.

Tang, Y., Carmichael, G. R., Kurata, G., Uno, I., Weber, R. J., Song, C. H., Guttikunda, S. K., Woo, J. H., Streets, D. G., Wei, C., and Clarke, A. D.: Impacts of dust on regional tropospheric chemistry during the ACE-Asia experiment: A model study with observations, J. Geophys. Res.-Atmos., 109, https://doi.org/10.1029/2003JD003806, 2004.

Tie, X., Madronich, S., Walters, S., Edwards, D. P., Ginoux, P., Mahowald, N., Zhang, R., Lou, C., and Brasseur, G.: Assessment of the global impact of aerosols on tropospheric oxidants, J. Geophys. Res.-Atmos., 110, https://doi.org/10.1029/2004JD005359, 2005.

Twomey, S.: Influence of pollution on shortwave albedo of clouds, J. Atmos. Sci., 34, 1149–1154, 1977.

Wang, J., Wang, S., Jiang, J., Ding, A., Zheng, M., Zhao, B., Wong, D. C., Zhou, W., Zheng, G., Wang, L., and Pleim, J. E.: Impact of aerosol–meteorology interactions on fine particle pollution during China's severe haze episode in January 2013, Environ. Res. Lett., 9, 094002, https://doi.org/10.1088/1748-9326/9/9/094002, 2014.

Wang, J., Allen, D. J., Pickering, K. E., Li, Z., and He, H.: Impact of aerosol direct effect on East Asian air quality during the EAST-AIRE campaign, J. Geophys. Res.-Atmos., 121, https://doi.org/10.13016/M27W0S, 2016.

Wang, J., Zhao, B., Wang, S., Yang, F., Xing, J., Morawska, L., Ding, A., Kulmala, M., Kerminen, V. M., Kujansuu, J., and Wang, Z.: Particulate matter pollution over China and the effects of control policies, Sci. Total Environ., 584–585, 426–447, 2017.

Wong, D. C., Pleim, J., Mathur, R., Binkowski, F., Otte, T., Gilliam, R., Pouliot, G., Xiu, A., Young, J. O., and Kang, D.: WRF-CMAQ two-way coupled system with aerosol feedback: software development and preliminary results, Geosci. Model Dev., 5, 299–312, https://doi.org/10.5194/gmd-5-299-2012, 2012.

Xing, J., Zhang, Y., Wang, S., Liu, X., Cheng, S., Zhang, Q., Chen, Y., Streets, D. G., Jang, C., Hao, J., and Wang, W.: Modeling study on the air quality impacts from emission reductions and atypical meteorological conditions during the 2008 Beijing Olympics, Atmos. Environ., 45, 1786–1798, 2011.

Xing, J., Mathur, R., Pleim, J., Hogrefe, C., Gan, C. M., Wong, D. C., Wei, C., and Wang, J.: Air pollution and climate response to aerosol direct radiative effects: a modeling study of decadal trends across the northern hemisphere, J. Geophys. Res., 120, 12221–12236, 2015a.

Xing, J., Mathur, R., Pleim, J., Hogrefe, C., Gan, C.-M., Wong, D. C., and Wei, C.: Can a coupled meteorology–chemistry model reproduce the historical trend in aerosol direct radiative effects over the Northern Hemisphere?, Atmos. Chem. Phys., 15, 9997–10018, https://doi.org/10.5194/acp-15-9997-2015, 2015b.

Xu, J., Zhang, Y.-H., Fu, J. S., Zheng, S., and Wang, W.: Process analysis of typical summertime ozone episodes over the Beijing area, Sci. Total Environ., 399, 147–157, 2008.

Xu, J., Zhang, Y. H., Zheng, S. Q., and He, Y. J.: Aerosol effects on ozone concentrations in Beijing: a model sensitivity study, J. Environ. Sci., 24, 645–656, 2012.

Yu, S., Mathur, R., Pleim, J., Wong, D., Gilliam, R., Alapaty, K., Zhao, C., and Liu, X.: Aerosol indirect effect on the grid-scale clouds in the two-way coupled WRF–CMAQ: model description, development, evaluation and regional analysis, Atmos. Chem. Phys., 14, 11247–11285, https://doi.org/10.5194/acp-14-11247-2014, 2014.

Zhang, Y., Wen, X. Y., Wang, K., Vijayaraghavan, K., and Jacobson, M. Z.: Probing into regional O_3 and particulate matter pollution in the United States: 2. An examination of formation mechanisms through a process analysis technique and sensitivity study, J. Geophys. Res.-Atmos., 114, https://doi.org/10.1029/2009JD011900, 2009.

Zhao, B., Wang, S., Dong, X., Wang, J., Duan, L., Fu, X., Hao, J., and Fu, J.: Environmental effects of the recent emission changes in China: implications for particulate matter pollution and soil acidification, Environ. Res. Lett., 8, 024031, https://doi.org/10.1088/1748-9326/8/2/024031, 2013a.

Zhao, B., Wang, S., Wang, J., Fu, J. S., Liu, T., Xu, J., Fu, X., and Hao, J.: Impact of national NO_x and SO_2 control policies on particulate matter pollution in China, Atmos. Environ., 77, 453–463, 2013b.